



# DYNAMIC ANALYSIS OF AN ANNULAR CAVITY: CRITERIA FOR THE SELECTION OF THE MODAL BASIS

J.-S. GENOT AND F. CHARRON

*Department of Mechanical Engineering, University of Sherbrooke, Sherbrooke,  
Québec, Canada J1K 2R1*

*(Received 14 January 1998, and in final form 17 July 1998)*

The study of the dynamic behavior of a structure coupled with a light fluid and excited by an external harmonic mechanical force needs a good understanding of the interaction between the solid and the fluid. As the fluid is not directly excited, the dynamic response of the fluid in the cavity depends only on the reciprocal influence of both media. This paper quantifies the fluid–structure interaction, as function of both the modal spatial coincidence between the solid and the fluid, and the frequency coincidence of the natural frequencies of both media with respect to the excitation frequency of the force. A simple method of comparison is developed to investigate the optimal contents of the modal basis. This makes the dynamic response of the cavity and the structure converge with a minimum number of modes. In order to address this problem, one has to develop criteria for defining the appropriate modes for each basis. The theory has been applied to four cases and the results show good agreement. Finally, some results are also compared with those obtained by a finite element model to demonstrate the usefulness of these criteria to find the optimal mesh size for both media.

© 1999 Academic Press

## 1. INTRODUCTION

Most of real life engineering problems involve interactions between two or more media. These problems are either external or internal. This paper, is concerned with internal problems involving closed cavities. For the last couple of decades, new numerical approaches used with the finite element method (FEM) have paved the way for a good understanding of coupled systems [1, 2]. A good review was made by Atalla and Bernhard [3]. Many applications are found in aeronautics and transport vehicles in view of reducing internal noise: in 1982, Nefske *et al.* [4] studied the finite element analysis of an automobile passenger compartment, in 1992 Green [5] proposed the vibroacoustic analysis of the Saab 2000 aircraft. Unfortunately, they were using empirical rules to fine the modal basis contents of both media. Consequently, the mesh size is not optimized. In theory it is very difficult to access the contents of each modal basis to ensure the convergence of the solution because coupled systems interact. Cacciolati *et al.* [6] and Lesueur [7] have proposed a criterion based on modal coincidence to differentiate the influence

of each mode on the response. They have applied this criterion to infinite and finite cylinders. However, they did not extend their results to the selection of the optimum modal contents. This paper aims to remedy the situation for a basic two-dimensional coupled system, which is a ring filled with a light fluid. The ring is excited with a point external force over a given frequency range. We will show that it is possible to predict the optimal mesh size of the cavity and the structure given the modal basis contents of the solid and fluid media. In practice, the ring model is valid for cylinders of great length as regards to their diameter: for example, passenger cabin of aircrafts and gas tanks [7, 8]. For such cases, longitudinal modes of the cavity do not couple with the radial and circumferential modes.

The ring displacement and the cavity pressure depend on four factors: the spatial coincidence of the force vector with the structure eigenmodes (modal participation factor), the modal coupling between the eigenmodes of both media, the frequency coincidence between the structure natural frequencies and the excitation frequency, and finally, the frequency coincidence between the cavity natural frequencies and the excitation frequency. The use of analytical mode shapes in a finite element formulation allows one to define a criterion for the definition of the modal contents of each medium and, thus, it becomes possible to identify the cavity and structure mode contribution to the dynamic responses of the coupled system given the maximum excitation frequency. As a consequence, the optimal mesh size of the ring and the fluid can be obtained because it is closely related to the wavelength of the selected modes. In general, it is recommended that at least 5 to 6 linear elements be used per wavelength.

Therefore, the major point of this work is the determination of the optimal (i.e., minimal) contents of the fluid modal basis. The mesh size of the fluid is closely related to these contents. In comparison, the search for optimal modal contents of the ring is easily resolved, because the light fluid does not influence its mode shapes and eigenfrequencies.

Section 2 presents the model and the general assumptions and focuses on the analytical approximation of both modal bases. Section 3 deals with the development of criteria for selecting the optimal contents of the modal basis. Section 4 makes use of these criteria in four cases taken from industrial examples. This section demonstrates their applicability for finite element analysis.

## 2. MODEL

### 2.1. GENERAL ASSUMPTIONS

The ring characteristics are shown in Figure 1. The ring is supposed to be perfect, which means the radius  $R$  and the thickness  $h$  are assumed constant. Thin shell theory is valid because the ring wall thickness is less than 10% of the radius. The width of the ring is negligible with regard to other dimensions so that no structure or cavity mode can appear along the longitudinal axis of the ring. This point is very important, because one can further ignore any possible coupling between longitudinal modes and radial modes. This work is also confined to

materials that are commonly used for ducts, containers, aircrafts or submarines, such as steel, aluminum, and some categories of composites like carbon fibers with a resin matrix. These materials share approximately the same longitudinal velocity of sound  $c_1$  which is about 5300 m/s. The longitudinal velocity of sound as a function of the material properties is

$$c_1 = \sqrt{\frac{E}{\rho_s(1 - \nu^2)}}, \quad (1)$$

where  $E$  stands for the Young's modulus (Mpa),  $\nu$  is the Poisson's ratio and  $\rho_s$  ( $\text{kg/m}^3$ ) is the density of the ring.

The ring is submitted to an external point force which is normal to the surface. Let  $r$  and  $\varphi$  be respectively the radial and angular co-ordinates of any point in the ring cross-section, and  $R$  and  $\varphi_0$  the co-ordinates of the point where the force is applied (see Figure 1).

## 2.2. APPROXIMATION OF THE SOLID AND FLUID MODAL BASES

In this section, the modal bases of both media are investigated. The bases are used in later sections to develop optimum modal contents criteria. Since the fluid/ring system is very simple, the mode shapes (ring and fluid) can be approximated with an equivalent analytical model where the number of degrees of freedom is reduced to two for the solid (displacements in the cross-sectional plane), and to one for the fluid (pressure).

### 2.2.1. Modal basis of the ring in vacuo

The mode shapes of the ring coupled with a *light* fluid are not differing very much from the mode shapes of the ring *in vacuo*. These mode shapes are solutions of a set of partial differential equations. There is not a general agreement in the

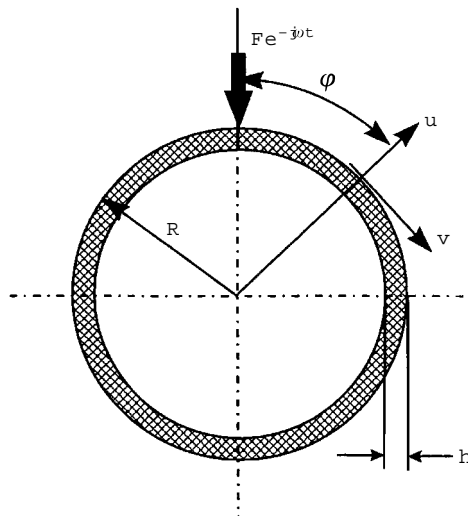


Figure 1. The model.

literature on the linear partial differential equations which describe the motions of the ring *in vacuo*. The differences among the theories are due to the various assumptions which are used in the formulation. A complete study and additional references can be found in reference [9]. For the purpose of simplicity, Love's equations have been chosen to illustrate the method but in fact, the Donell's equations were used for the computations:

$$\frac{Eh^3}{12R^4} \left( \frac{\partial^2 v}{\partial \varphi^2} - \frac{\partial^3 w}{\partial \varphi^3} \right) + \frac{Eh}{R^2} \left( \frac{\partial^2 v}{\partial \varphi^2} + \frac{\partial w}{\partial \varphi} \right) = \rho_s h \frac{\partial^2 v}{\partial t^2}, \quad (2)$$

$$\frac{Eh^3}{12R^4} \left( \frac{\partial^3 v}{\partial \varphi^3} - \frac{\partial^4 w}{\partial \varphi^4} \right) + \frac{Eh}{R^2} \left( \frac{\partial v}{\partial \varphi} + w \right) = \rho_s h \frac{\partial^2 w}{\partial t^2} + F^d, \quad (3)$$

where  $v$  is the tangential displacement and  $w$  the radial displacement (see Figure 1). Eigenfrequencies  $\omega_s^i$  and eigenvectors  $\phi_s^i$  of the ring are solutions of equations (2) and (3) with no external force ( $F^d = 0$ ). One is looking for these solutions in the form of either the so called symmetric vector (equation (4)) or in the form of its antisymmetric counterpart (equation (5)):

$$\{\bar{\phi}_s^i\} = \begin{pmatrix} A_v \sin(i\varphi) \\ A_w \cos(i\varphi) \end{pmatrix}, \quad \{\phi_s^i\} = \begin{pmatrix} -A_v \cos(i\varphi) \\ A_w \sin(i\varphi) \end{pmatrix}. \quad (4, 5)$$

The symmetric and antisymmetric mode shapes differ from one another by a rotation of  $\pi/2i$ . If  $i$  equals zero, the ring has a so called extensional mode which consists in a purely radial deformation. The existence of two solutions for the same integer  $i$  is called a degenerescence. This phenomenon is only valid for perfect geometry of revolution, so it does not exist in real problems. By choosing the same angular reference ( $\varphi = \varphi_0 = 0^\circ$ ) for the force and the mode shapes,  $[\phi_s^i]^T \{F^d\}$  is equal to zero for the symmetric vector. Therefore, *one can only consider the antisymmetric solution*. One substitutes equation (5) into equations (2) and (3) to get the system of equations

$$\begin{bmatrix} i^2 - \lambda_s^2 & i \\ i & 1 + \gamma^2 i^4 - \lambda_s^2 \end{bmatrix} \begin{Bmatrix} A_v \\ A_w \end{Bmatrix} = \begin{Bmatrix} 0 \\ 0 \end{Bmatrix}, \quad (6)$$

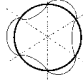
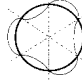
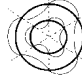
$$\lambda_s^2 = \rho_s (1 - \nu^2) R^2 w^2 / E = R^2 \omega^2 / c_1^2, \quad \gamma = h/R\sqrt{12}. \quad (7, 8)$$

The determinant of the matrix of equation (6) is set to zero in order to obtain the non-trivial solutions which produce a fourth order polynomial in  $\lambda_s$ :

$$(\lambda_{s\pm}^i)^2 = \frac{1}{2} \left[ (1 + i^2 + \gamma^2 i^4) \pm \sqrt{(1 + i^2)^2 + 2\gamma^2 i^4 (1 - i^2) + \gamma^4 i^8} \right]. \quad (9)$$

The two possible signs stand for the two families of mode shapes: the so called extensional modes are related to the  $+$  sign, and the flexural modes are related to the  $-$  sign (see Tables 1 and 2, and Blevins [9] for more details). The first two values of the flexural modes  $\lambda_{s-}^i$ , i.e.,  $\lambda_{s-}^0$  and  $\lambda_{s-}^1$ , are generally not considered because they almost equal zero. This means that the first flexural mode begins with

TABLE 1  
*Synthesis of the eigenmodes of the system*

Type	Structure	Fluid
Circumferential (symmetric and antisymmetric)		
Radial	Order $i$ None	Order $m$ 
Eigenvectors (symmetric and antisymmetric)	Flexural — $\phi_{s-}^i$ Extensional — $\phi_{s+}^i$	Order $k$ $\phi_j^{(m,k)}$
Eigenvalues (symmetric and antisymmetric)	Flexural — $\omega_{s-}^i$ Extensional — $\omega_{s+}^i$	$\omega_j^{(m,k)}$

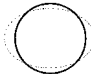
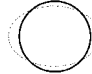
$i = 2$ . This is not the case for the extensional modes.  $\lambda_{s+}^0$  is related to the so called ring frequency, which corresponds to a pure radial deformation, and  $\lambda_{s+}^1$  characterizes the solid-body movement. Equation (9) shows that extensional modes (sign +) have greater eigenfrequencies than flexural modes (sign -) which can be easily explained by the difference in energy that each type of mode requires to produce the same displacement.

Finally, the  $i$ th eigenfrequency of the ring is given by

$$(\omega_{s\pm}^i)^2 = \frac{c_1^2(\lambda_{s\pm}^i)^2}{R^2}. \tag{10}$$

Blevins [9] gives approximate relations for  $\lambda_{s\pm}^i$ . Furthermore, Blevins omits the term  $\gamma^4 i^8$  in equation (9), but it can be proven to be relatively important for high

TABLE 2  
*Differences between the extensional and flexural modes*

	Flexural modes	Extensional modes
Mode shape		
Stress	Radial	Tangential
Natural frequencies	$\omega_{s+}^i > \omega_{s-}^i$	

values of  $i$ . Once the eigenfrequencies are solved, the system (equation 6) gives the ratio of  $A_v$  over  $A_w$  (see equation (11)). Here again, extensional modal amplitudes are related to the  $+$  sign, and flexural ones to the  $-$  sign. For  $i = 0$  (extensional modes only), the ratio is unknown but it is still possible to calculate the modal response using the equation of the modal mass normalization (see equation (14) later in this section):

$$\frac{A_{v\pm}}{A_{w\pm}} = \frac{i}{(\lambda_{s\pm}^i)^2 - i^2}, \quad \text{for } i \neq 0. \tag{11}$$

Finally, one substitutes equation (11) into equation (5) for the two possible signs of  $\lambda_s^i$ , and the antisymmetric vectors are put in the form

$$\{\phi_{s-}^i\} = A_{w-} \begin{pmatrix} \frac{i}{(\lambda_{s-}^i)^2 - i^2} \sin(i\varphi) \\ \cos(i\varphi) \end{pmatrix}, \quad \text{for the antisymmetric flexural modes,} \tag{12}$$

$$\{\phi_{s+}^i\} = A_{w+} \begin{pmatrix} \frac{i}{(\lambda_{s+}^i)^2 - i^2} \sin(i\varphi) \\ \cos(i\varphi) \end{pmatrix}, \quad \text{for the antisymmetric extensional modes.} \tag{13}$$

It is a common practice to normalize the eigenmodes with respect to the mass. By equating  $m_s^i$  to unity, an explicit form of  $A_{w+}$  and  $A_{w-}$  can be obtained:

$$m_{s\pm}^i = \int_{\Omega_s} \rho_s |\{\phi_{s\pm}^i\}|^2 d\Omega_s = 1, \tag{14}$$

$$A_{w\pm} = (\rho_s \pi R h L)^{-1/2} \left[ 1 + \frac{i^2}{(\lambda_{s\pm}^i)^2 - i^2} \right]^{-1/2}, \quad \text{for } i \neq 0, \tag{15}$$

$$A_{w+} = (2\rho_s R h L)^{-1/2}, \quad \text{for } i = 0. \tag{16}$$

### 2.2.2. Modal basis of the fluid

For the fluid, the cavity is studied using the Helmholtz’s formula in cylindrical co-ordinates (equation (17)) and a boundary condition stipulating that for the structure bounding the fluid, the particle velocity normal to the surface is equal to the normal velocity of the surface (equation (18)). If the fluid is supposed to move freely the last formula is replaced by the rigid wall boundary condition

(equation (19)). In fact, the eigenmodes of the fluid are solutions of equations (17) and (19), where  $p$  represents the pressure inside the ring:

$$\left( \frac{\partial^2}{\partial r^2} + \frac{\partial^2}{r^2 \partial \varphi^2} + \frac{\partial}{r \partial r} \right) p = 0, \quad (17)$$

$$\left( \frac{\partial p}{\partial r} \right)_{r=R} = -\rho_s \frac{\partial^2 w}{\partial t^2}, \quad \left( \frac{\partial p}{\partial r} \right)_{r=R} = 0. \quad (18, 19)$$

As for the ring, there is a symmetric and an antisymmetric mode for each eigenfrequency. If the phase angle between the fluid and the ring is set to zero, one only needs the antisymmetric component

$$\phi_f^{(m,k)} = BJ_m \left( \frac{\lambda_f^{(m,k)} r}{R} \right) \cos(m\varphi), \quad (20)$$

where  $J_m$  is the Bessel function of the first kind of order  $m$ , and  $\lambda_f^{(m,k)}$  is the  $k$ th solution of  $J'_m(\lambda_f) = 0$ . For more information about these functions, see references [8, 10, 11]. The fluid eigenfrequency is related to  $\lambda_f^{(m,k)}$  by

$$(\omega_f^{(m,k)})^2 = \frac{c^2 (\lambda_f^{(m,k)})^2}{R^2}. \quad (21)$$

The modal pattern of the pressure is defined by two integers:  $m$  refers to the number of nodal points along the tangential axis and  $k$  refers to the number of nodal points along the radial axis (see Table 1).

Here again, the modal mass of the fluid can be set to 1 and from the previous equations, the value of  $B$  is given by:

$$m_f^{(m,k)} = \frac{1}{\rho_f c^2} \int_{\Omega_f} (\phi_f^{m,k})^2 d\Omega_f = 1, \quad (22)$$

$$B = \left( \frac{2\rho_f c^2}{\pi R^2 L} \right)^{-1/2} \beta_{(m,k)}^{-1/2}, \quad \text{for } m \geq 1, \quad (23)$$

$$B = \left( \frac{\rho_f c^2}{\pi R^2 L} \right)^{-1/2} \beta_{(0,k)}^{-1/2}, \quad \text{for } m = 0, \quad (24)$$

where  $\beta_{(m,k)} = J_m^2(\lambda_f^{(m,k)}) - J_m(\lambda_f^{(m,k+1)})J_m(\lambda_f^{(m,k-1)})$ .

### 3. DEVELOPMENT OF CRITERIA FOR MODE SELECTION

In this section, we want to develop simple methods to best define the optimal modal basis (fluid and structure) without altering the accuracy of the dynamic

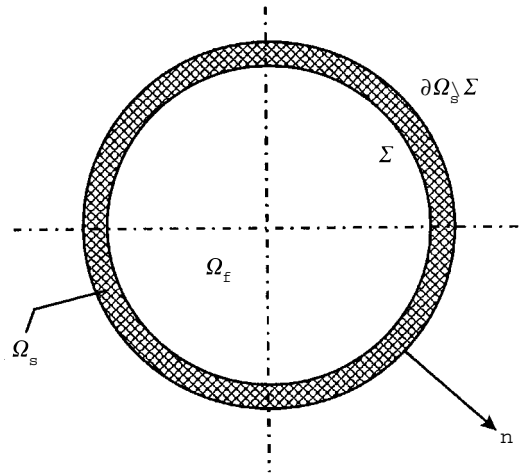


Figure 2. Domain definition.

response throughout the frequency range of the excitation ( $0-\omega_m$ ). One can approach this in two stages: first, one finds the maximum *circumferential orders* of the solid and the fluid thanks to the modal displacements of the system. Since it is not enough to further find the maximum *radial order*  $k$  of the fluid, one uses some global indicators for the cavity to evaluate it. The quadratic pressure integrated over the entire fluid domain is a good indicator for internal stationary problems.

### 3.1. FLUID AND RING MODAL DISPLACEMENTS

In this paper, the internal fluid is assumed light and homogeneous. The definition of the domains for each medium is shown in Figure 2. The discretized form of the vibro-acoustic equation is given by Morand and Ohayon [2]:

$$\left( -\omega^2 \begin{bmatrix} [M] & [0] \\ [D]^T & [K_p] \end{bmatrix} + \begin{bmatrix} [K] & -[D] \\ [0] & [H] \end{bmatrix} \right) \begin{Bmatrix} \{U\} \\ \{P\} \end{Bmatrix} = \begin{Bmatrix} \{F^d\} \\ \{0\} \end{Bmatrix}, \tag{25}$$

where  $\{U\}$  is the nodal displacement vector of the ring,  $\{P\}$  the nodal pressure vector of the fluid,  $\{F^d\}$  the external force acting on the ring,  $[M]$  and  $[K]$  the mass and stiffness matrices of the ring,  $[K_p]$  and  $[H]$  matrices resulting from the discretization of pressure integrals, and  $[D]$  a coupling matrix. At this stage, it is possible to introduce the dissipation effect using a structural damping model for both media. Real matrices  $[K]$  and  $[H]$  are replaced by their complex equivalent:

$$[K] \leftrightarrow (1 + j\eta_s)[K], \quad [H] \leftrightarrow (1 + \xi\eta_f)[H], \tag{26, 27}$$

where it is assumed that  $\eta_s$  and  $\eta_f$  are independent of the frequency. In order to reduce the size of the system of equations given in equation (25), displacement and pressure are projected in the uncoupled modal basis:

$$\{U\} = [\phi_s]\{q_s\}, \quad \{P\} = [\phi_f]\{q_f\}, \tag{28, 29}$$



where  $[\phi_s] = [\{\phi_s^1\}, \{\phi_s^2\}, \dots, \{\phi_s^{n_s}\}]$  is the matrix of the first  $n_s$  eigenvectors of the structure,  $[\phi_f] = [\{\phi_f^1\}, \{\phi_f^2\}, \dots, \{\phi_f^{n_f}\}]$  is the matrix of the first  $n_f$  eigenvectors of the fluid, and equations (28) and (29) are substituted in equation (25) to give

$$-\omega^2 \begin{bmatrix} [\phi_s]^T[M][\phi_s] & [0] \\ [\phi_s]^T[D]^T[\phi_f] & [\phi_f]^T[K_p][\phi_f] \end{bmatrix} + \dots$$

$$\begin{bmatrix} [\phi_s]^T[K][\phi_s] & -[\phi_s]^T[D][\phi_f] \\ [0] & [\phi_f]^T[H][\phi_f] \end{bmatrix} \begin{Bmatrix} \{q_s\} \\ \{q_f\} \end{Bmatrix} = \begin{Bmatrix} [\phi_s]^T\{F^d\} \\ \{0\} \end{Bmatrix}. \quad (30)$$

As the fluid is supposed to be light compared to the ring, it hardly contributes to the response of the structure. Consequently, the term standing for the fluid participation in equation (30) is negligible:

$$([\phi_s]^T[D][\phi_f])\{q_f\} \ll [\phi_s]^T\{F^d\}. \quad (31)$$

In practice, equation (31) must be carefully checked before any further calculation is made. To the authors' knowledge, there is no analytical criterion to check the validity of the light-fluid hypothesis in the case of cylinders. In his work, Scott [12] uses the flat-plate fluid-loading criterion of Crighton [13]. However, this criterion is not really appropriate for cylinders.

In the case of no acoustic sources in the cavity, the structure is driving the generation of pressure in the cavity. Consequently, the displacement and pressure dynamic responses can be computed from

$$([\phi_s]^T[K][\phi_s] - \omega^2[\phi_s]^T[M][\phi_s])\{q_s\} = [\phi_s]^T\{F^d\}, \quad (32)$$

$$([\phi_f]^T[H][\phi_f] - \omega^2[\phi_f]^T[K_p][\phi_f])\{q_f\} - \omega^2[\phi_s]^T[D]^T[\phi_f]\{q_s\} = 0. \quad (33)$$

After some manipulations, the components of the modal pressure vector of the ring are shown to be

$$q_s^i(\omega) = \frac{\{\phi_s^i\}^T\{F^d\}}{m_s^i((\omega_s^i)^2 - \omega^2 + j\eta_s(\omega_s^i)^2)}, \quad (34)$$

where  $m_s^i$  is the ring modal mass of mode  $i$ ,  $\{\phi_s^i\}$  the ring eigenvector of mode  $i$  *in vacuo*, and  $\omega_s^i$  the ring eigenfrequency of mode  $i$ . Analog calculations for the fluid give

$$q_{f\pm}^{(m,k)} = \frac{\omega^2}{(\omega_f^{(m,k)})^2 - \omega^2 + j\eta_f(\omega_f^{(m,k)})^2} \cdot \left( \sum_{i=1}^N d_{\pm}^{(m,k,i)} \frac{\Gamma_{\pm}^i}{(\omega_{s\pm}^i)^2 - \omega^2 + j\eta_s(\omega_{s\pm}^i)^2} \right), \quad (35)$$

where

$$\Gamma_{\pm}^i = \{\phi_{s\pm}^i\}^T\{F^d\}. \quad (36)$$

In these equations,  $j$  is equal to  $\sqrt{-1}$ . In equation (35), the modal coupling matrix is written  $[d]$  for clarity (with  $[d] = [\phi_s]^T[D]^T[\phi_f]$ ). It is noticed that a deep understanding of the problem cannot be achieved without the introduction of

damping, and the damping factors mainly affect the amplitude of the response in the neighborhood of the eigenfrequencies.

In equations (34) and (35), the modal coupling factor  $d^{(m,k,i)}$  and the modal participation factor  $\Gamma_{\pm}^i$  are expressed as function of the modes approximations. Explicitly, one has

$$d_{\pm}^{(m,k,i)} = \int_{\Sigma} \langle \phi_f^{(m,k)} \rangle \{ \phi_{s\pm}^i \} \cdot \{ n \} \, d\Sigma, \quad (37)$$

where  $\{n\}$  is the normal surface vector with unit modulus, and  $\Sigma$  is the internal surface of the ring (i.e., the surface in contact with the fluid). The orthogonality of functions  $\sin(i\varphi)$  and  $\sin(m\varphi)$  implies that the modal coupling is zero unlike when  $i$  equals  $m$ . In other words, the coupling condition requires ring and fluid circumferential mode shape patterns to be the same. After some manipulations, equation (37) yields for  $i \geq 1$  and  $i = m$ :

$$d_{\pm}^{(m,k,i)} = d_{\pm}^{(i,k)} = \left( \frac{2\rho_f c^2}{\rho_s R h} \right)^{1/2} \lambda_f^{(i,k)} ((\lambda_f^{(i,k)})^2 - i^2)^{-1/2} \left( 1 + \frac{i^2}{((\lambda_{s\pm}^i)^2 - i^2)^2} \right)^{-1/2}. \quad (38)$$

For  $i = 0$ , the modal coupling factor reduces to  $\sqrt{2rFc^2/\rho_s R h}$ . We have also defined a nondimensional coupling factor for the only purpose of graphical convenience:

$$\mathcal{D}_{\pm}^{(m,k,i)} = \mathcal{D}_{\pm}^{(i,k)} = \lambda_f^{(i,k)} ((\lambda_f^{(i,k)})^2 - i^2)^{-1/2} \left( 1 + \frac{i^2}{((\lambda_{s\pm}^i)^2 - i^2)^2} \right)^{-1/2}. \quad (39)$$

For  $i = 0$ , the non-dimensional modal coupling factor equals 1. As a consequence of the equality of the fluid and solid circumferential mode order, the modal pressure does not have a sum over  $i$  any longer. Equation (35) now reads

$$q_{f\pm}^{(i,k)} = \frac{\omega^2}{(\omega_f^{(m,k)})^2 - \omega^2 + j\eta_f(\omega_f^{(m,k)})^2} \cdot d_{\pm}^{(k,i)} \cdot \frac{\Gamma_{\pm}^i}{(\omega_{s\pm}^i)^2 - \omega^2 + j\eta_s(\omega_{s\pm}^i)^2}. \quad (40)$$

The modal participation factor is expressed in terms of continuous functions:

$$\Gamma_{\pm}^i = \int_{\Sigma} \{ F^d \} \cdot \{ \phi_{s\pm}^i \} \, d\Sigma, \quad \Gamma_{\pm}^i = F_0 A_{w\pm} \cos(i\varphi_0), \quad (41, 42)$$

where it is noted that  $\varphi_0$  has been set to 0. Equations (15) and (16) are used to define a nondimensional form of the dynamic factor:

$$\mathcal{G}_{\pm}^i = \left[ 1 + \frac{i^2}{((\lambda_{s\pm}^i)^2 - i^2)^2} \right]^{-1/2}, \quad \text{for } i \neq 0, \quad (43)$$

and

$$\mathcal{G}_{\pm}^i = 1, \quad \text{for } i = 0. \quad (44)$$

### 3.2. THE OPTIMAL MODAL BASIS OF THE RING

First, two assumptions are noted: the ring is negligibly influenced by the fluid and the ring is directly excited by the force. As a consequence, the choice of the modal basis is only directed by the number of structural antisymmetric modes that fall in the frequency range of the force. It is reasonable to retain the first  $i$ th eigenfrequencies that are less than  $\omega_m$  (upper value of the frequency). The highest value of  $i$  is named  $i_m$  and it defines the optimal mesh size for the solid. It also defines the optimal circumferential mesh size for the fluid,  $m_m = i_m$ , as shown in the calculation of the modal coupling factor (section). *If the fluid is heavy, these conclusions do not hold*, because the fluid contributes to the solid movement.

There are two types of orders  $i$ : extensional and flexural. As already mentioned, eigenfrequencies of extensional modes are higher than eigenfrequencies of flexural modes. Thus the modal density in the range  $[0-\omega_m]$  (rad/s) is greater for flexural modes. Consequently, *the flexural modes* give the upper value of  $i$ . Blevins [9] gives an approximate formula for  $i$  as a function of the physical parameters of the system and the maximum excitation frequency. When  $i_m$  is much less than  $R/h$  and greater than 3, one has

$$i_m = \text{Int} \left[ \sqrt{\frac{R\omega_m}{\gamma c_1}} \right], \quad (45)$$

where in the Blevin's formula, one sets  $\omega = \omega_m$  to find  $i_m$ .

### 3.3. THE QUADRATIC PRESSURE IN THE FLUID

The modal pressure  $q_{f\pm}^{(m,k)}$  does not give any information about the upper value of the radial order  $k$  of the fluid. A good criterion would investigate the convergence of the pressure as function of  $k$ , within the complete frequency range of the excitation.

In fact, one is not interested in the pressure at every point in the cavity but in a more global indicator. In the context of finite elements applications, the quadratic pressure is a good global vibroacoustic indicator because its convergence depends on the modal contents only. Other indicators like the acoustic intensity seem to be less attractive because the convergence also depends on the phase shift between pressure and velocity. Furthermore, these indicators are more often used in the context of external problems. Another approach could be a total integration over space and frequency. Unfortunately, as convenient as it seems (one scalar variable), this approach hides a lot of information and cannot be treated analytically.

The quadratic pressure is equal to the weighted sum of pressure over the fluid volume. Equation (46) gives the total quadratic pressure when it is truncated at

orders  $K-$  and  $I-$  for the flexural modes, and  $K+$  and  $I+$  for the extensional modes:

$$\begin{aligned} \langle p_{(I\pm, K\pm)}^2(\omega) \rangle &= \frac{1}{\Omega_f} \int_{\Omega_f} \left( \sum_{k=0}^{K-} \sum_{i=2}^{I-} \phi_f^{(i,k)} q_{f-}^{(i,k)} \right) \left( \sum_{k=0}^{K-} \sum_{i=2}^{I-} \phi_f^{(i,k)} q_{f-}^{(i,k)} \right)^* d\Omega_f \\ &+ \dots + \frac{1}{\Omega_f} \int_{\Omega_f} \left( \sum_{k=0}^{K+} \sum_{i=0}^{I+} \phi_f^{(i,k)} q_{f+}^{(i,k)} \right) \left( \sum_{k=0}^{K+} \sum_{i=0}^{I+} \phi_f^{(i,k)} q_{f+}^{(i,k)} \right)^* d\Omega_f. \end{aligned} \tag{46}$$

The values of integers  $I\pm$  and  $K\pm$  are chosen such that the quadratic pressure converges. The search for the best values of  $I\pm$  and  $K\pm$  makes the central point of this paper. One has already seen that  $I-$  and  $I+$  can be found if one keeps only the first  $i$ th eigenfrequencies (in fact,  $I-$  for flexural modes directs the discretization of the ring). Substituting equations (14), (22), (38) and (42) into equation (35), and then into equation (46), the final form of the mean quadratic pressure is given by

$$\begin{aligned} \langle p_{(I\pm, K\pm)}^2(\omega) \rangle &= \frac{\rho_f c^2}{\pi R^2 L} \sum_{k=0}^{K-} \sum_{i=2}^{I-} \left( \frac{\omega^4}{H_f(\omega)} \right) (d_{-}^{(i,k)})^2 \left( \frac{(\Gamma_{-}^i)^2}{H_s(\omega)} \right) \\ &+ \dots + \frac{\rho_f c^2}{\pi R^2 L} \sum_{k=0}^{K+} \sum_{i=0}^{I+} \left( \frac{\omega^4}{H_f(\omega)} \right) (d_{+}^{(i,k)})^2 \left( \frac{(\Gamma_{+}^i)^2}{H_s(\omega)} \right), \end{aligned} \tag{47}$$

where  $H_f(\omega) = ((\omega_f^{(i,k)})^2 - \omega^2)^2 + \eta_f^2 (\omega_f^{(i,k)})^4$  and  $H_s(\omega) = ((\omega_s^i)^2 - \omega^2)^2 + \eta_s^2 (\omega_s^i)^4$ . The mean quadratic pressure is now used to find the optimal modal basis of the fluid.

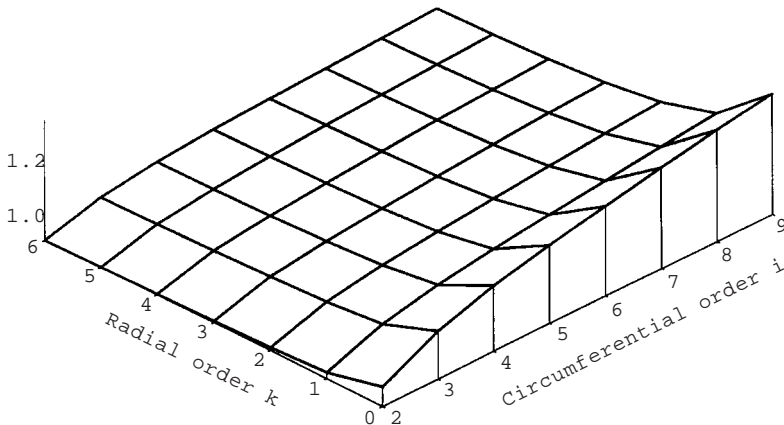


Figure 3. Non-dimensional modal coupling  $\mathcal{D}_{-}^{(i,k)}$ , flexural modes.

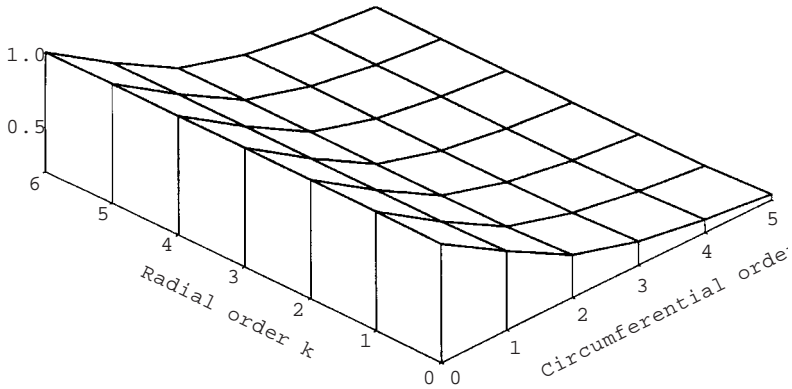


Figure 4. Non-dimensional modal coupling  $\mathcal{G}_+^{(i,k)}$ , extensional modes.

### 3.4. THE OPTIMAL MODAL BASIS OF THE FLUID

#### 3.4.1. Introduction

In equation (47), some terms are dependent on the orders  $k$  and  $i$  and others are constant for given dimensions of the ring. By taking a closer look at both types of terms, one concludes the following.

The  $\mathcal{D}_-^{(i,k)}$  term is not a function of  $\omega$ , and it really takes no part in the selection of modes, because it evolves slowly when  $i$  or  $k$  increases (see Figure 3). The same remark applies to  $\mathcal{G}_-$  (see Figure 5). Consequently, flexural modes are selected by the frequency coincidence only.

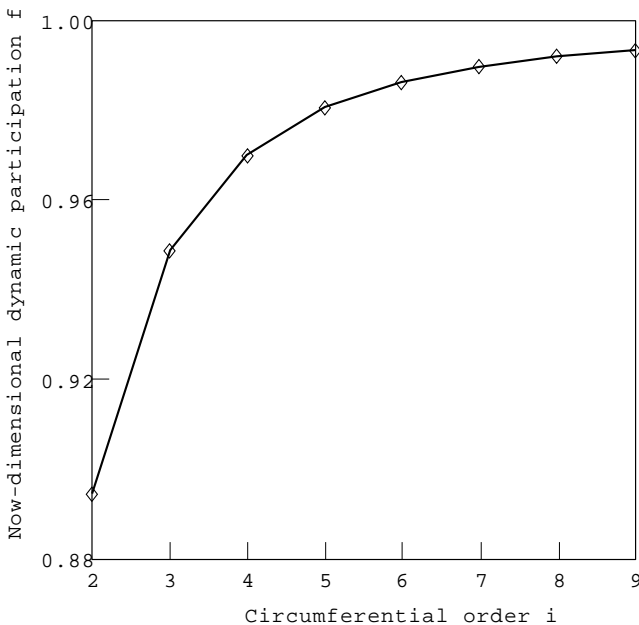


Figure 5. Non-dimensional dynamic participation factor  $\mathcal{G}_-$ , flexural modes:  $\diamond$ , points of simulation.

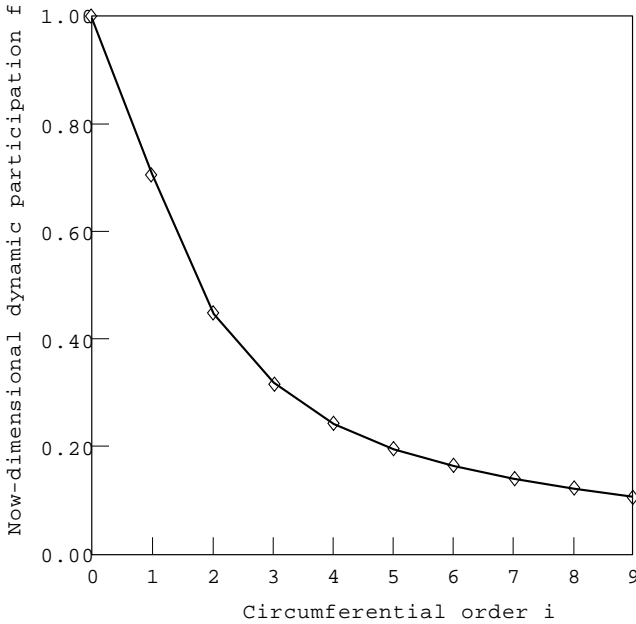


Figure 6. Non-dimensional dynamic participation factor  $\mathcal{G}_+$ , extensional modes:  $\diamond$ , points of simulations.

The  $\mathcal{D}_+^{(i,k)}$  term evolves quite differently. Figure 4 shows that for low circumferential orders  $i$ , the non-dimensional modal coupling term is larger than for higher values of the circumferential order (whatever the radial order). This conclusion is to be noted for the subsequent parts. The same remark applies to  $\mathcal{G}_+$  (Figure 6).

As a consequence, these terms do not help to find the optimal basis of the fluid.

One defines now the partial mean quadratic pressure response of the fluid for the given orders  $i$  and  $k$  (equation (48)), regardless of the type of mode (either extensional or flexural). One will see later that the partial quadratic pressure plays a great role in the determination of the maximum radial order:

$$\begin{aligned} \langle p_{(i,k)}^2(\omega) \rangle &= \frac{\rho_f c^2}{\pi R^2 L} \left( \frac{\omega^4}{((\omega_f^{(i,k)})^2 - \omega^2)^2 + \eta_f^2 (\omega_f^{(i,k)})^4} \right) (d^{(i,k)})^2 \\ &\quad \times \left( \frac{(\Gamma^i)^2}{((\omega_s^i)^2 - \omega^2)^2 + \eta_s^2 (\omega_s^i)^4} \right). \end{aligned} \tag{48}$$

The total quadratic pressure (equation (47)) is the sum of partial quadratic pressures over  $k$  and  $i$ . If  $\langle p_{i,k}^2(\omega) \rangle$  is drawn versus frequency (say from 0 to  $\omega_m = 2\pi \times 500$  rad/s), the partial pressure reaches maxima as  $\omega$  enters the neighborhoods of either  $\omega_f^{(i,k)}$  or  $\omega_s^i$ , unless  $\omega_f^{(i,k)}$  or  $\omega_s^i$  are greater than 500 Hz.

Calculations show that conclusions about the optimal radial order ensuring convergence are quite different whether fluid eigenfrequencies are falling inside  $[0 - \omega_m]$  or not. The following paragraphs outline the main results.

### 3.4.2. First case: fluid eigenfrequencies are greater than $\omega_m$

One is looking first for the geometry conditions that cause all the fluid eigenfrequencies to be higher than  $\omega_m$ . The eigenfrequencies of the fluid are given by equation (21). For any given circumferential mode  $i$ , the lowest fluid eigenfrequency happens for  $k = 0$ . Consequently, the radius for which the fluid eigenfrequencies are larger or equal to  $\omega_m$  is given by

$$R_1 = \frac{\lambda_f^{(i,0)} c}{\omega_m}. \quad (49)$$

The value of  $R_1$  is obtained by setting  $i = 2$  for flexural modes. In theory, extensional modes of the ring should be considered too. However, one demonstrates easily that inequalities  $\omega_{s+}^i \leq \omega_m$  and  $\omega_f^{(i,0)} \geq \omega_m$  are antithetic. Consequently, extensional modes are not considered in this paragraph.

Once the value of  $R_1$  is known, step two consists in finding the radial order  $k_f$  which ensures convergence of the mean quadratic pressure. Intensive simulations show (see section 3.4.4) that the highest error levels are always to be found at the solid eigenfrequencies. Thus, the convergence study will focus on these frequencies (i.e.,  $\omega = \omega_{s-}^i$ , for any  $i$ ). Let  $j$  be one particular circumferential order of solid. When  $\omega = \omega_{s-}^j$  and assuming a low modal density, other circumferential orders  $i \neq j$  do not take part in the convergence process. Consequently, the mean quadratic pressure becomes (flexural modes only are included)

$$\langle p_{(l-,K-)}^2(\omega_{s-}^j) \rangle = \frac{\rho_f c^2}{\pi R^2 L} \frac{1}{\eta_s^2} \sum_{k=0}^{K-} (d_{-}^{(j,k)})^2 (\Gamma_{-}^j)^2 \frac{1}{((\omega_{f}^{(j,k)})^2 - (\omega_{s-}^j)^2)^2 + \eta_f^2 (\omega_{f}^{(j,k)})^4}. \quad (50)$$

Each solid eigenfrequency of order  $i$  couples with an infinity of fluid eigenfrequencies bearing the same  $i$  and any value of  $k$  between 0 and  $\infty$ . For one particular  $j$  inside 2 and  $i_m$ , the contribution of successive radial orders to the *final* mean quadratic pressure (equation (50)) is given by the terms of the series. As they are positive, the mathematical properties of the series (rate of convergence) are simply inferred from the properties of each term (partial quadratic pressures). For  $k = 0$ , the partial quadratic pressure  $\langle p_{(2,0)}^2(\omega_{s-}^j) \rangle$  is taken as a common reference. For any  $k > 0$ ,  $\langle p_{(j,k)}^2(\omega_{s-}^j) \rangle$  is compared with the reference using a partial mean quadratic pressure contribution factor  $\tau_j(k)$ . This indicator is given

$$\tau_j(k) = \frac{\langle p_{(j,k)}^2(\omega_{s-}^j) \rangle}{\langle p_{(2,0)}^2(\omega_{s-}^j) \rangle}. \quad (51)$$

Minor calculations using equation (48) show that  $\tau_i(k)$  can simplify to

$$\tau_j(k) = \left( \frac{\omega_{s-}^2}{\omega_{s-}^j} \right)^4 \left( \frac{(1 - \mu_{(2,0)}^2)^2 + \eta_f^2 \mu_{(2,0)}^4}{(1 - \mu_{(j,k)}^2)^2 + \eta_f^2 \mu_{(j,k)}^4} \right), \quad (52)$$

with

$$\mu_{(j,k)} = \frac{\omega_f^{(j,k)}}{\omega_{s-}^j}. \quad (53)$$

The factor  $\tau_j(k)$  and  $\mu_{(j,k)}$  are rewritten to take account of the explicit forms of the radial natural frequencies  $\omega_j^{(j,k)}$  and  $\omega_{s-}^j$ . One finds that

$$\tau_j(k) = \left( \frac{\lambda_{s-}^2}{\lambda_j^2} \right)^4 \left( \frac{(1 - \mu_{(2,0)}^2)^2 + \eta_f^2 \mu_{(2,0)}^4}{(1 - \mu_{(j,k)}^2)^2 + \eta_f^2 \mu_{(j,k)}^4} \right), \tag{54}$$

with

$$\mu_{(j,k)} = \frac{c}{c_1} \frac{\lambda_f^{(j,k)}}{\lambda_{s-}^j}. \tag{55}$$

As  $c$  and  $c_1$  are assumed constant (the material properties are given),  $\mu_{(j,k)}$  varies with the ratio  $R/h$  only and  $\lambda_{s-}^2/\lambda_{s-}^j$ . As a consequence,  $\tau_j(k)$  also varies with  $R/h$  only.

This remark allows one to plot  $\tau_j(k)$  versus  $k$  for multiple values of  $R/h$ . For  $R/h > 10$ , simulations show that *the contribution factor does not really depend on  $R/h$* . Another possible influent parameter could be the damping factor. Here again, the contribution factor does not vary for common values of damping (less than 0.7).

In Figure 7, the contribution factor is plotted for several values of  $j$  and one particular value of the ratio  $R/h$ . It is noticed that the convergence is governed by the lowest  $j$ . Consequently, the maximum radial order  $k$  is chosen by means of the highest curve, i.e.,  $j = i$ . In many cases,  $k = 2$  ensures a 95% convergence. It is clear that rings having a very high number of excited modes will not require higher values of  $k$  to make the quadratic pressure converge.

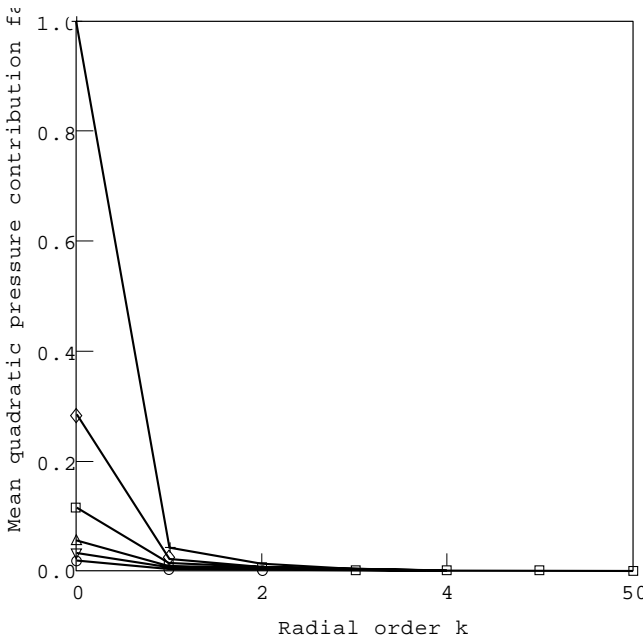


Figure 7. Typical mean quadratic pressure contribution factor  $\tau_j(k)$ . Note:  $\tau_j(k)$  is almost independent of  $R$ ,  $\eta_f$ , and  $\eta_s$ , and for  $R/h > 10$ ,  $\tau_j(k)$  is fairly independent of the value of  $R/h$ : +,  $j = 2$ ;  $\diamond$ ,  $j = 3$ ;  $\square$ ,  $j = 4$ ;  $\triangle$ ,  $j = 5$ ;  $\nabla$ ,  $j = 6$ ;  $\circ$ ,  $j = 7$ .



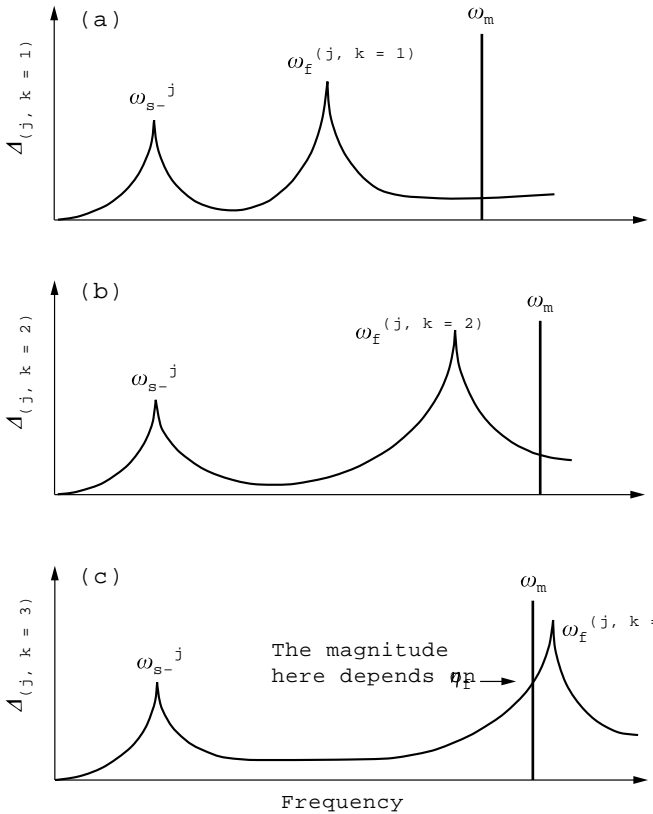


Figure 8. Evolution of the error as  $k$  increases. In (a) and (b) the first two eigenfrequencies of the fluid coupled with the solid of same circumferential order  $j$  take substantial part in the pressure error. In (c), the third fluid eigenfrequency is rejected after the maximum excitation frequency, thus playing no role in the error; the error moves towards high frequencies.

3.4.3. *Second case: fluid eigenfrequencies are less than  $\omega_m$*

The radius for which the lowest fluid mode ( $k = 0$ ) couples to a flexural solid mode ( $i = 2$ ) is given by

$$R_2 = \frac{\lambda_f^{(2,0)} c}{\omega_m} . \tag{56}$$

Nonetheless, if the radius is increased enough (equation (57)), there are also extensional modes in the frequency range. As a result, equation (57) also gives the radius for which every type of modes is inside  $[0-\omega_m]$ :

$$R_3 = \frac{c_1}{\omega_m} . \tag{57}$$

First, one considers there is no extensional mode between 0 and  $\omega_m$ . For the purpose of simplicity, one assumes that there is only the first flexural eigenfrequency of the ring lying between 0 and  $\omega_m$ . Let  $j$  be the corresponding value of  $i$  ( $j = 2$  for flexural modes). The condition for effective coupling between the structure and the cavity shows that each structure eigenfrequency of order  $j$

can couple with an infinite number of fluid eigenfrequencies which bear the same value of  $j$ , regardless of the value of  $k$ . For  $i = j$ , the eigenfrequencies of the fluid that are able to couple with  $\omega_{s-}^j$  are  $\omega_f^{(j,k)}$  where  $k = 0, 1, \dots, \infty$ . For convenience, it is supposed that among all the fluid frequencies,  $\omega_f^{(j,k=0)}$ ,  $\omega_f^{(j,k=1)}$  and  $\omega_f^{(j,k=2)}$  are less than  $\omega_m$ . It should be remembered that they are not prone to direct resonance with the external force. One focuses now on the global pressure which is a sum of partial pressures. In this case,  $I- = j$ , and equation (47) reduces to

$$\langle p_{(I-,K-)}^2(\omega) \rangle = \frac{\rho_f c^2}{\pi R^2 L} \sum_{k=0}^{K-} \left( \frac{\omega^4}{H_f(\omega)} \right) (d^{(j,k)})^2 \left( \frac{(\Gamma_-^j)^2}{H_s(\omega)} \right). \tag{58}$$

To give a good idea of the convergence rate of the global pressure as function of order  $K-$  (but it also applies whatever the type of mode, that is why the letter  $K$  without a subscript is employed in equations (59) and (60)), one plots the following successive differences as function of frequency in Figure 8:

$$\begin{aligned} \Delta_{(j,1)}(\omega) &= \langle p_{(I=j,K=1)}^2(\omega) \rangle - \langle p_{(I=j,K=0)}^2(\omega) \rangle \\ &= \langle p_{(I=j,k=1)}^2(\omega) \rangle, \end{aligned} \tag{59}$$

$$\begin{aligned} \Delta_{(j,2)}(\omega) &= \langle p_{(I=j,K=2)}^2(\omega) \rangle - \langle p_{(I=j,K=1)}^2(\omega) \rangle \\ &= \langle p_{(I=j,k=2)}^2(\omega) \rangle, \end{aligned} \tag{60}$$

and so on.  $\Delta_{(j,k)}(\omega)$  is directly related to the partial quadratic pressure. As shown in Figure 8, the difference is locally distributed around the fluid and solid eigenfrequencies. The convergence rate is then strictly dependent on the number of fluid and solid eigenmodes that are less than  $\omega_m$ . In particular, the eigenfrequency of the fluid remains a source of noticeable error as long as  $\omega_f^{(j,k)} \leq \omega_m$ . When this source disappears (i.e.,  $k$  is large enough to make the local difference vanish (in this example, it happens for  $k = 2$ )), the error changes place and reaches a new level at the eigenfrequency  $\omega_{s-}^j$  of the solid. The smallest value of  $k$  that satisfies  $\omega_f^{(j,k)} \geq \omega_m$  is  $k_f$  ( $f$  for flexural).

When there is more than one solid mode in  $[0-\omega_m]$ , the choice of  $j$  to calculate  $k_f$  is simple. Each particular  $j$  between 2 and  $i_m$  gives a new value of  $k_f$ . Among all these different radial orders, the upper one is the final  $k_f$ . However, it is possible to demonstrate that  $j = 2$  still gives the final value in a straightforward way. From

TABLE 3  
*Basic dimensions for the four simulated rings*

Case	$R/h$	$R$ (m)
1 (low damping)	150	0.2
2 (low damping)	110	1.1
3 (low damping)	20	1.4
4 (high damping)	20	1.4

Blevins [9], one knows  $\omega_j^{(i,k)}$  is an increasing function of  $i$  and  $k$ . For the first values of  $i$  and  $k$ , one has

$$\omega_j^{(i,k)} \simeq Ai + Bk + C, \quad (61)$$

with  $A = (\pi c)/(2R)$ ,  $B = (\pi c)/R$  and  $C = (\pi c)/(4R)$ . Consequently, the upper value of  $k_f$  is obtained for  $i = j = 2$  which is the lowest value of  $i$  (for flexural modes).

Two further remarks need to be made. First, as long as there are no extensional modes excited by the driving force, one takes  $j = 2$  to calculate  $k_f$ . Otherwise, it is better to take  $j = 0$  (because the smallest circumferential order for the extensional modes is 0). As a consequence, the presence of extensional modes can slightly increase  $k_f$  (by not more than about one unit). Second, all fluid eigenfrequencies for which  $k > k_f$  are greater than  $\omega_m$ . For these modes, it all comes down to the case for which fluid modes are falling off the frequency range (section 3.4.2). It is then possible to refine the convergence study. The same contribution factor  $\tau_i(k)$  can be used, starting with  $k = k_f$  in place of  $k = 0$  (that is,  $k_f$  is the new reference of the refined convergence study). However, in most cases, the convergence is found to be very good without any refinement (see section 3.4.4).

#### 3.4.4. Summing up

The main results are as follows.

If  $R \leq R_1$ , there are only flexural solid eigenfrequencies in  $[0-\omega_m]$ . First, one calculates  $i_m$  with equation (45), and gives oneself a certain error level in percent. Second, the upper value of the radial order is found with the help of the contribution factor  $\tau$  in Figure 7. Furthermore, in most cases,  $k = 2$  is largely sufficient to reach error levels less than 5% in mean quadratic pressure.

If  $R \geq R_2$  and  $R \leq R_3$ , there are flexural modes and fluid eigenfrequencies in  $[0-\omega_m]$ . The upper value of  $k$  should not exceed  $k_f$ . The order  $k_f$  is the radial order of the maximum eigenfrequency of the fluid in  $[0-\omega_m]$  for  $i = 2$ , plus one. A good approximation of  $k_f$  when it is greater than 1 is given by

$$k_f = \text{Int} \left[ \frac{R\omega_m}{\pi c - \frac{5}{4}} \right] + 1. \quad (62)$$

If  $R\omega_m/(\pi c - \frac{5}{4})$  is negative, one sets  $k_f = 0$ . It is possible to further refine the convergence study with the contribution factor (see section 3.4.3).

If  $R > R_3$ , for large diameters, extensional modes are also excited. One takes  $i = 0$  in place of  $i = 2$  to calculate  $k_f$  (equation (63)):

$$k_f = \text{Int} \left[ \frac{R\omega_m}{\pi c - \frac{1}{4}} \right] + 1. \quad (63)$$

TABLE 4

*The first natural frequencies of the fluid (Hz)*

	Case 1		Case 2		Case 3 or 4	
	$i = 0$	$i = 2$	$i = 0$	$i = 2$	$i = 0$	$i = 2$
$k = 0$	0	905	0	161	0	118
$k = 1$	1135	1987	188	318	148	259
$k = 2$	2079	2955	345	475	271	385
$k = 3$	3015	3903	500	632	393	509
$k = 4$	3950	4845	655	789	515	631
$k = 5$	4882	5783	810	946	636	754

## 4. VALIDATION

## 4.1. THE MODELS

The results of section 3 are checked computing the global quadratic pressure in a ring, by means of equation (46). The circumferential orders  $I+$  and  $I-$  have been systematically set to  $i_m$  (for  $I+$ , it is largely over-evaluated but it does not matter except from a computational point of view). High values of  $K+$  and  $K-$ , 8 for example, ensure the convergence of the mean quadratic pressure, thus giving what is called the final mean quadratic pressure. Intermediate values of the mean quadratic pressure  $0 < K_{\pm} < 8$  are calculated and compared to the final mean

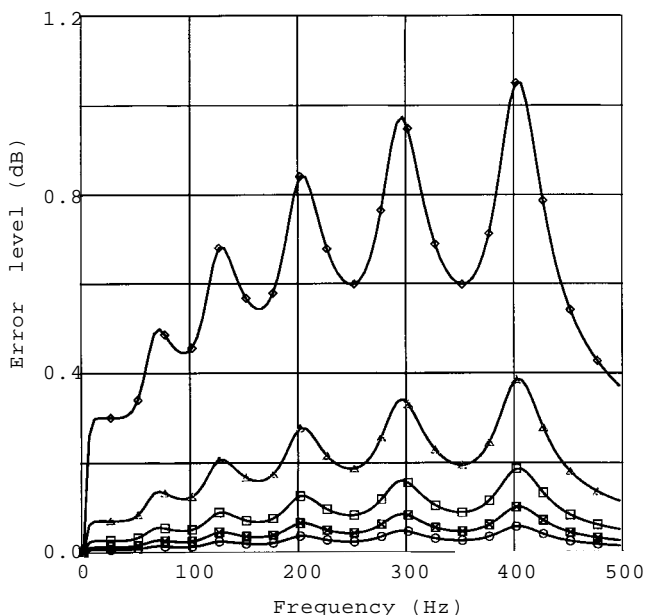


Figure 9. Case 1, error level for successive values of  $K$ , flexural and extensional modes:  $\diamond$ ,  $k = 0$ ;  $\triangle$ ,  $k = 1$ ;  $\square$ ,  $k = 2$ ;  $\boxtimes$ ,  $k = 3$ ;  $\circ$ ,  $k = 4$ .

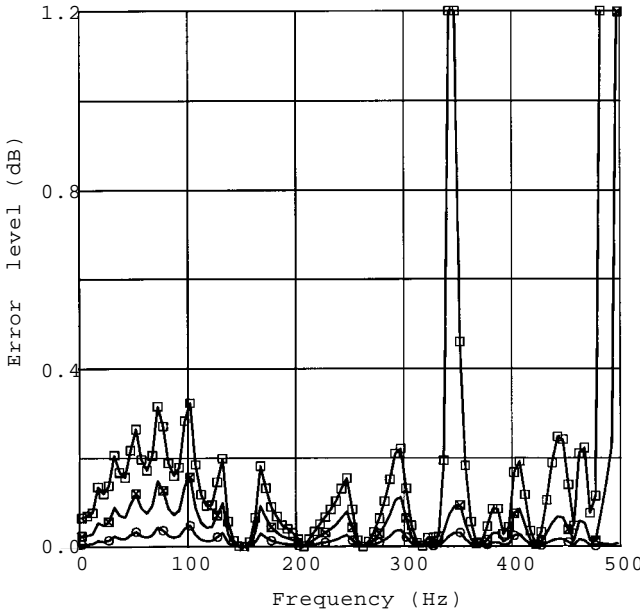


Figure 10. Case 2, error level for successive values of  $K$ , flexural and extensional modes:  $\square$ ,  $k = 2$ ;  $\boxtimes$ ,  $k = 3$ ;  $\circ$ ,  $k = 4$ .

quadratic pressure ( $K_{\pm} = 8$ ). The error is drawn in dB by taking the final mean quadratic pressure as a reference:

$$\text{error for } K = 20 \times \log \left( \frac{\text{mean quadratic pressure for } K < 8}{\text{final mean quadratic pressure for } K = 8} \right). \quad (64)$$

The error level is computed for extensional and flexural modes separately. Four cases have been investigated. The ratios of  $R/h$  and  $R$  vary as shown in Table 3. They allow to change the fluid modal density, thus changing the values of  $k_f$  (see Table 4). Low and high damping factors refer to the values taken on by  $\eta_s$  and  $\eta_f$ ; low damping:  $\eta_s = 0.05$ ,  $\eta_f = 0.01$ ; high damping:  $\eta_s = 0.5$ ,  $\eta_f = 0.1$ .

The physical properties of the ring and the fluid are:  $c_1 = 5440$  m/s,  $\rho_f = 1.28$  kg/m<sup>3</sup>,  $E = 210 \times 10^9$  N/m<sup>2</sup>,  $c = 340$  m/s,  $\rho_s = 7800$  kg/m<sup>3</sup>,  $L = 0.02$  m.

The length of the ring is 0.02 m. This value allows one to decouple the circumferential displacements from the longitudinal displacements. The external force is 2 N and the upper frequency of excitation is  $\omega_m = 2\pi \times 500$  rad/s. The computational tasks have been performed with MATLAB.

Figures 9–12 show the error level of the quadratic pressure for  $K = 0$  to 4, and for all four cases. We have first treated the flexural and extensional modes *separately* for each of the four cases using equation (64), and then superimposed both types of modes (see Figures 9 to 12).

The second step consisted of carrying out a finite element analysis (FEA) of one of the aforementioned models, with MSC-NASTRAN. The analyst must be aware that the FEA software takes the angular phase between the solid and the fluid at random, whereas the same angle has been set to zero in this paper ( $\varphi = \varphi_0 = 0$ ).

Consequently, it is very difficult to compare analytical results with intermediate numerical results such as modal pressures. Other major limitations of the finite element method concern the way the pressure or the displacements are approximated over each element. For this paper, our models were using linear elements. The fluid is represented by hexahedral elements with 8 corner nodes. At the center of the cavity, hexahedral elements are replaced by pentahedral elements. The ring structure is represented by linear plate elements. The plate elements are constrained along the  $x$ -axis as shown in Figure 13.

Only results for case 2 will be presented. For case 2, the finite element software is run three times with an increasing number of nodes in the radial direction each time: 5, 15 and 25 nodes. These numbers of nodes are sufficient to represent properly the radial cavity mode orders  $k$  of 0, 2 and 4, respectively. All structure modes between 0 and 500 Hz and all fluid modes between 0 and 2000 Hz have been kept for the analysis. The 0–500 Hz interval corresponds to the domain of excitation frequencies. The second interval, 0–2000 Hz, is deduced from the maximum frequency of the fluid that influences the response. In fact, it is  $\omega_f^{(i,k)}$  for  $i = i_m$  and  $k = k_f$ .

#### 4.2. COMPARISON WITH THE THEORY

The four cases have been chosen for various reasons. In case 1, only flexural eigenmodes are less than  $\omega_m$ . In case 2, there are flexural solid and fluid eigenmodes in  $[0-\omega_m]$ . In cases 3 and 4, all modes are present, but their damping factor varies.

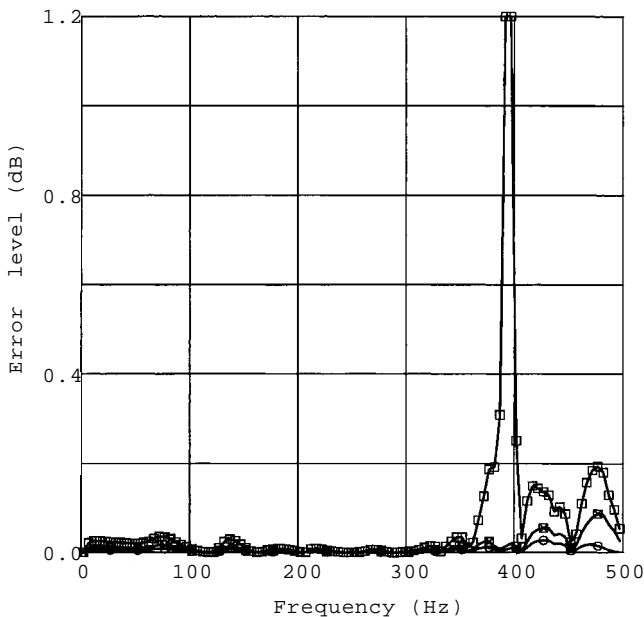


Figure 11. Case 3, error level for successive values of  $K$ , flexural and extensional modes:  $\square$ ,  $k = 2$ ;  $\boxtimes$ ,  $k = 3$ ;  $\circ$ ,  $k = 4$ .

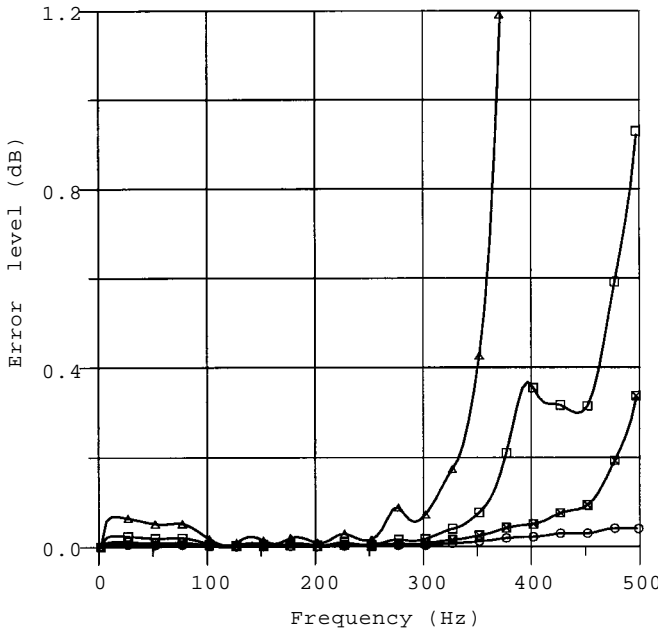


Figure 12. Case 4, error level for successive values of  $K$ , flexural and extensional modes:  $\triangle$ ,  $k = 1$ ;  $\square$ ,  $k = 2$ ;  $\boxtimes$ ,  $k = 3$ ;  $\circ$ ,  $k = 4$ .

For case 1, Figure 7 gives the upper value of  $k$ . For cases 2, 3 and 4, equations (62) and (63) have been used for the computation of the theoretical upper values of  $k_f$ . This scheme gives the results presented in Table 5.

#### 4.2.1. Analytical cases

In case 1 (Figure 9), the error level remains lower than 0.5 dB (less than 6% of relative error in mean quadratic pressure) for  $K = 1$  between 0 and 500 Hz. As a result,  $k = 1$  ensures good convergence. The theoretical value for  $k_f$  is 1 (see Table 5).

In case 2, the presence of fluid eigenmodes gives much higher mean quadratic pressure levels than case 1 for localized frequencies (the frequencies that are closest to fluid and solid eigenfrequencies). From Figure 10,  $K = 2$  is a good choice to make the pressure converge up to 94%. Equation (62) would have given  $k_f = 4$ , showing that the theoretical value of  $k_f$  is a conservative value depending if some fluid modes are significantly contributing or not to the mean quadratic pressure.

In case 3, extensional modes are included. This case highlights that extensional modes do not play a great role in the convergence process because they couple much less efficiently with the fluid than with flexural modes. The proper radial order  $k_f$  can be calculated either by taking  $i = 2$  or  $i = 0$  (if one wants to take account of extensional modes) in equation (63). The theoretical value for  $k_f$  is 3 for flexural modes and 4 for extensional modes. From Figure 11,  $K = 3$  is a good choice to make the pressure converge to up to 0.1 dB.

Case 4 emphasizes the role of high damping factors. In particular, the peaks now overlap, and the modes are much less selective (compare Figure 11 with

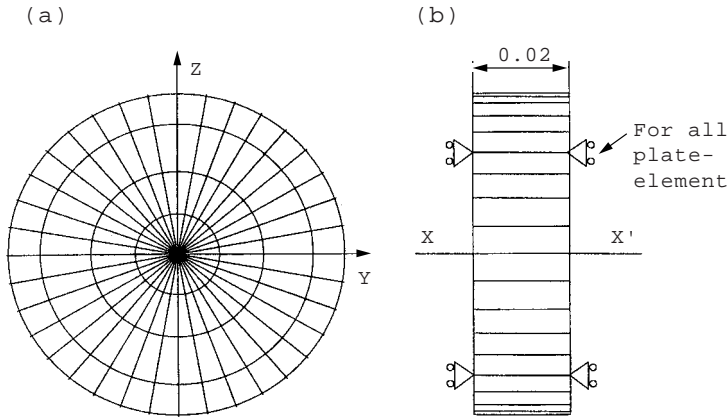


Figure 13. The finite element model: (a) meshing of the fluid, (b) meshing of the ring.

Figure 12). As a result, the extensional modes are gaining in importance (particularly those which are slightly greater than  $\omega_m$ ), leading to an increase of the value of  $k_f$ . Another effect of high damping is to reduce the mean error level, hence a wrong value of  $k_f$  will not drastically affect the global precision. Finally, one could think that both phenomena compensate—the effect of extensional modes and the drop in error level due to high damping—so there is no need to change  $k_f$ . However, this is not a general remark. The theoretical value for  $k_f$  is 3 for flexural modes and 4 for extensional modes. From Figure 12,  $K = 3$  is a good choice to make the pressure converge to up to 0.3 dB.

#### 4.2.2. Finite element analysis

As expected, the finite element analysis gives very similar conclusions about  $k_f$ . Only results for case 2 are presented. Figures 14 and 15 show the superimposition of the quadratic pressure for 5 and 25 nodes per radius, and for 15 and 25 nodes per radius, respectively. It corresponds to the comparison of  $K = 0$  and  $K = 4$  with  $K = 2$  and  $K = 4$ . The mesh refinement makes the error of the finite element analysis decrease in the full range of frequencies, especially near the highest frequency 500 Hz. For 15 nodes per radius (which suggests taking  $k_f \geq 3$ ) the convergence seems to be almost reached, according to analytical predictions.

TABLE 5  
Theoretical values of  $k_f$  for the  
four cases

	Case 1	Case 2	Case 3 or 4
$i = 2$	$k_f = 0$	$k_f = 3$	$k_f = 3$
$i = 0$	$k_f = 1$	$k_f = 4$	$k_f = 4$



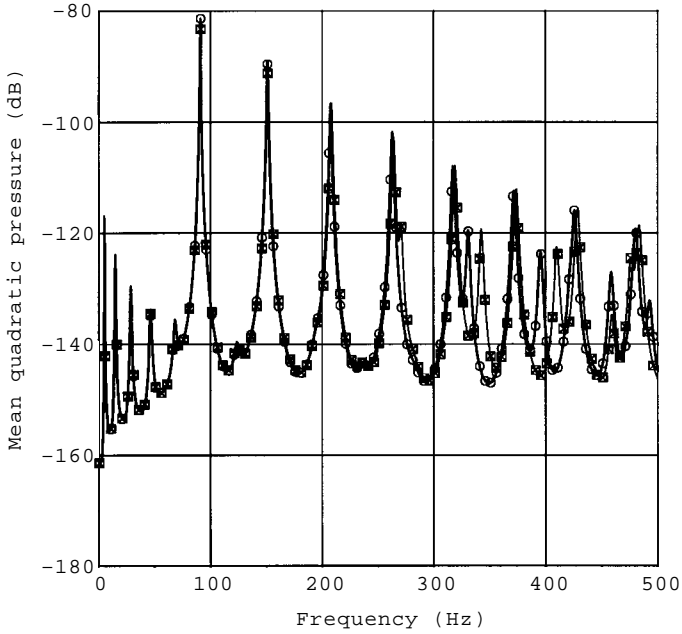


Figure 14. Mean quadratic pressure (dB):  $\circ$ , 25 nodes in radial direction;  $\boxtimes$ , 5 nodes in radial direction.

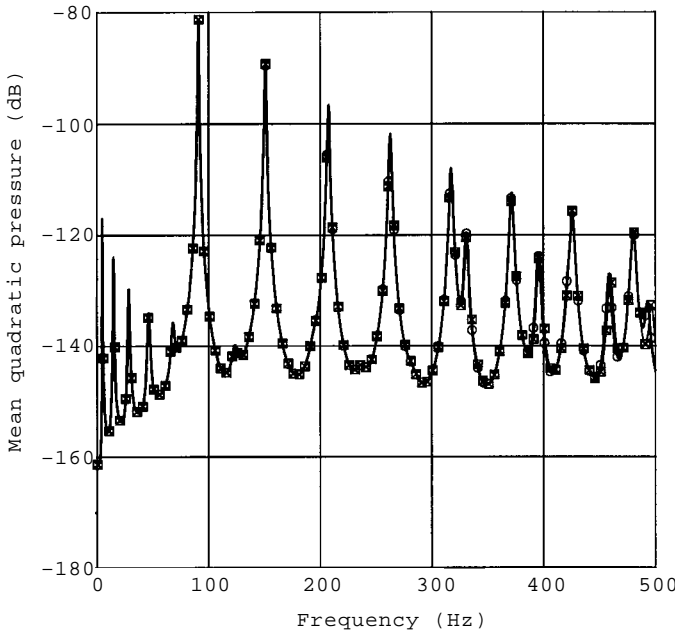


Figure 15. Mean quadratic pressure (dB):  $\circ$ , 25 nodes in radial direction;  $\boxtimes$ , 15 nodes in radial direction.

## 5. SYNTHESIS

Here, a final synthesis of the last sections is briefly presented. All numbers are given for materials with  $c_1 \simeq 5300$  m/s.

For small diameters ( $\leq 0.60$  m approximately) and  $R/h > 10$ , the upper value of  $k$  should be less than 2. The best value is given by Figure 7: this value depends on  $i_m$  (i.e., on the radius). It should be noted that  $i_m$  is the maximum circumferential order of the flexural solid eigenmodes. A good approximation of  $i_m$  when  $i_m$  is much less than  $R/h$  and greater than 3 (see reference [9]) is given by

$$i_m = \text{Int} \left[ \sqrt{\frac{R\omega_m}{\gamma c_1}} \right]. \quad (65)$$

For midsize diameters (between 0.6 and 2.6 m approximately) and  $R/h > 10$ , the upper value of  $k$  should be less than  $k_f$ . The order  $k_f$  is the radial order of the maximum eigenfrequency of the fluid in  $(0-\omega_m)$  for  $i = 2$ . A good approximation of  $k_f$  when it is greater than 1 is given by

$$k_f = \text{Int} \left[ \frac{R\omega_m}{\pi c - \frac{5}{4}} \right] + 1. \quad (66)$$

If  $R\omega_m/(\pi c - \frac{5}{4})$  is negative,  $k_f = 0$ .

For large diameters ( $\geq 2.6$  m) and  $R/h > 10$ , the upper value of  $k$  should be less than  $k_f$ . The order  $k_f$  is the radial order of the maximum eigenfrequency of the fluid in  $(0-\omega_m)$  for  $i = 0$ . A good approximation of  $k_f$  when it is greater than 1 is given by

$$k_f = \text{Int} \left[ \frac{R\omega_m}{\pi c - \frac{1}{4}} \right] + 1. \quad (67)$$

If  $R\omega_m/(\pi c - \frac{1}{4})$  is negative,  $k_f = 0$ .

## 6. CONCLUSION

The first goal of the paper was to establish some criteria about the optimal modal contents. The addressed problem is limited to the ring filled with a light gas and externally excited with an external force. To the author's knowledge, no theoretical rule exists in the field so far. The second goal is to gain a deeper understanding of fluid-structure interaction for a structure with a perfect geometry. The ring study presents a lot of advantages: it is a basic and a relatively simple case of a coupled system and the number of variables is not too large.

The first step consisted of formulating the modal system of equations for a vibroacoustic problem. From these uncoupled modal equations, it is possible to obtain the circumferential order of the solid as well as radial and circumferential orders of the fluid. It is straightforwardly deduced that the circumferential orders of the two media must be equal to satisfy the

coupling condition. Consequently, the structure imposes its circumferential modal contents upon the fluid. As the element size of the structure is inversely proportional to the number of excited modes, the nodal circumferential mesh of the fluid is not unknown any longer. The previous system of equations provides no information about the radial order in the fluid. An energy-based criterion is needed to learn more about it. The second step uses the modal pressure to calculate the quadratic pressure in the cavity. The quadratic pressure is written in the form of a series involving the radial order of the fluid. Thus, the convergence of the quadratic pressure can be analyzed. The error level has proven to be the best tool. It has been shown that the fluid obeys a similar law as the structure: the radial mesh density is proportional to the modal contents of the fluid under the maximum frequency of excitation. The third step validates the previous results.

This work attempts to give some new criteria for the definition of the contents for modal basis and, indirectly, for the definition of meshing criteria for ring-cavity problems. The present case is very simple and does not directly address real applications. But, it prepares the study of more complex systems, particularly cylinders with light or heavy fluids, cylinders with imperfect geometries, or cylinders with uneven repartition of loadings.

#### REFERENCES

1. M. A. HAMDI and G. VERCHERY 1978 *Int. J. Num. Meth. Eng.* **13**, 139–150. A displacement method for the analysis of vibrations of coupled fluid–structure systems.
2. H. J.-P. MORAND and R. OHAYON 1992 *Interactions Fluides–Structures*. Masson.
3. N. ATALLA and R. J. BERNHARD 1994 *Applied Acoustics* **43**, 271–294. Review of numerical solutions for low-frequency structural-acoustic problems.
4. D. J. NEFSKE, JR, J. A. WOLF and L. J. HOWELL 1982 *Journal of Sound and Vibration* **80**, 247–266. Structural-acoustic finite element analysis of the automobile passenger compartment: a review of current practice.
5. I. S. GREEN 1992 In *4th NASA/SAE/DLR Aircraft Interior Noise Workshop*, 44–69. Vibro-acoustic FE analyses of the Saab 2000 aircraft.
6. C. CACCIOLATI, M. GOTTELAND and M. BARBE 1985 *Revue d'Acoustique* **72**, 92–101. Transmission d'énergie acoustique par une coque cylindrique finie excitée par des ondes planes externes.
7. C. LESUEUR 1988 *Rayonnement Acoustique des Structures*. Collection Département Etudes et Recherches EDF. Eyrolles.
8. M. HECKL 1957 *PhD Thesis* Shallabsstrahlung und Schalldämmung von Zylinderschalen.
9. R. D. BLEVINS 1987 *Formulas for Natural Frequency and Mode Shape*. Malabar, FL: Robert E. Krieger Publishing Company.
10. MCLACHLAN 1955 *Bessel Functions for Engineers*. Oxford University Press; 2nd edition.
11. P. W. SMITH 1957 *Journal of Acoustical Society of America* **29**, 721–729. Sound transmission through thin cylindrical shells.
12. J. F. M. SCOTT 1988 *Journal of Sound and Vibration* **125**, 241–280. The free modes of propagation of an infinite fluid-loaded thin cylindrical shell.
13. D. G. CRIGHTON 1980 *Journal of Sound and Vibration* **68**, 15–33. Approximations to the admittances and free wavenumbers of fluid-loaded panels.

## APPENDIX: NOMENCLATURE

$A$	magnitude coefficient of the analytical mode shape
$B$	Bessel function coefficient
$c$	speed of sound in the fluid (m/s)
$c_1$	speed of longitudinal waves in the ring (m/s)
$[D]$	fluid–structure coupling matrix
$d$	modal fluid–structure coupling
$\mathcal{D}$	a dimensional modal fluid–structure coupling
$E$	Young’s modulus (N/m <sup>2</sup> )
$F$	force (N)
$\mathcal{G}$	nondimensional modal participation factor
$h$	ring wall thickness (m)
$i$	circumferential mode (ring)
$i_m$	maximum circumferential mode
$I$	maximum (truncation) order for circumferential modes
$[H]$	fluid matrix
$j$	$\sqrt{-1}$
$J_m$	Bessel function (first kind) of order $m$
$k$	radial mode (fluid)
$k_f$	maximum radial mode
$k_s$	modal stiffness
$[K]$	stiffness matrix
$K$	maximum (truncation) order for radial modes
$[\bar{K}]$	stiffness matrix (real part) and structural damping matrix (imaginary part)
$[K_p]$	fluid matrix
$L$	length of the ring (m)
$m$	circumferential mode (fluid)
$m_s$	modal mass
$[M]$	mass matrix
$\{n\}$	unit normal vector to the surface of the ring, pointing outwards
$n_s$	number of structure modes
$n_f$	number of fluid modes
$\{P\}$	nodal pressure (finite element analysis)
$p$	real pressure (Pa)
$\{q_f\}$	modal pressure response of the fluid
$\{q_s\}$	modal displacement response of the ring
$R$	radius (m)
$\{U\}$	nodal displacement vector (FEM)
$\{u\}$	displacement vector (m)
$v$	tangential displacement (m)
$V_f$	volume of the fluid domain ( $\Gamma_f$ )
$w$	radial displacement (m)

*Greek letters*

$\alpha$	constant ( $0 < \alpha < 1$ )
$\beta$	constant ( $0 < \beta < 1$ )
$\epsilon$	strain
$\eta_f$	structural damping ratio (fluid)
$\eta_s$	structural damping ratio (solid)
$\gamma$	$h/R\sqrt{12}$
$\Gamma$	modal participation factor
$\nu$	Poisson ratio
$\lambda_s^i$	$i$ th eigenvalue coefficient of the ring

$\lambda_f^{(i,k)}$	eigenvalue coefficient of orders $i$ and $k$ of the fluid
$\mu$	fluid–structure eigenvalue ratio
$\omega$	frequency (rad/s)
$\omega_m$	maximum excitation frequency (rad/s)
$\{\phi_s\}$	ring eigenmode (or mode shape)
$\{\phi_f\}$	fluid eigenmode
$\Omega_f$	fluid domain
$\Omega_s$	solid domain
$\rho_s$	ring density ( $\text{kg/m}^3$ )
$\rho_f$	fluid density ( $\text{kg/m}^3$ )
$\sigma$	stress ( $\text{N/m}^2$ )
$\Sigma$	ring–fluid interface (surface)
$\tau$	partial mean quadratic pressure contribution factor
$\varphi$	angle (rad)
$\varphi_0$	angular position of the external force

*Subscripts*

$s$	structure
$f$	fluid
$+$	extensional modes
$-$	flexural modes
$\pm$	extensional and flexural modes

*Superscripts*

$i$	circumferential ring mode order
$n$	fluid mode order
$m$	circumferential fluid mode order
$k$	radial fluid mode order
$*$	complex conjugate
$T$	transpose of a matrix